Published in final edited form as:

Nat Med. 2009 October ; 15(10): 1186–1194. doi:10.1038/nm.2029.

Kcne2 deletion uncovers its crucial role in thyroid hormone biosynthesis

Torsten K. Roepke[1,*], **Elizabeth C. King**[1], **Andrea Reyna-Neyra**[2], **Monika Paroder**[2], **Kerry Purtell**[1], **Wade Koba**[3], **Eugene Fine**[3], **Daniel J. Lerner**[4], **Nancy Carrasco**[2], and **Geoffrey W. Abbott**[1,†]

[1]Greenberg Division of Cardiology, Department of Medicine and Department of Pharmacology, Weill Medical College of Cornell University, New York, NY

[2]Department of Molecular Pharmacology, Albert Einstein College of Medicine, The Bronx, NY

[3]M. Donald Blaufox MicroPet Lab for Molecular Imaging, Department of Nuclear Medicine, Albert Einstein College of Medicine, The Bronx, NY

[4]CV Ingenuity, San Francisco, CA.

Abstract

Thyroid dysfunction affects 1–4% of the population worldwide, causing defects including neurodevelopmental disorders, dwarfism and cardiac arrhythmia. Here, we show that KCNQ1 and KCNE2 form a TSH-stimulated, constitutively-active, thyrocyte K^+ channel required for normal thyroid hormone biosynthesis. Targeted disruption of *Kcne2* impaired thyroid iodide accumulation up to 8-fold, impaired maternal milk ejection and halved milk T_4 content, causing hypothyroidism, 50% reduced litter size, dwarfism, alopecia, goiter, and cardiac abnormalities including hypertrophy, fibrosis, and reduced fractional shortening. The alopecia, dwarfism and cardiac abnormalities were alleviated by T_3/T_4 administration to pups, by supplementing dams with T_4 pre- and postpartum, or by pre-weaning surrogacy with $Kcne2^{+/+}$ dams; conversely these symptoms were elicited in $Kcne2^{+/+}$ pups by surrogacy with $Kcne2^{-/-}$ dams. The data identify a critical thyrocyte K^+ channel, provide a possible novel therapeutic avenue for thyroid disorders, and predict an endocrine component to some previously-identified *KCNE2*- and *KCNQ1*-linked human cardiac arrhythmias.

Keywords

cardiac hypertrophy; hypothyroidism; KCNE2; KCNQ1; MiRP1; NIS; potassium channel; thyroid

†Address correspondence to: Dr. Geoffrey W. Abbott, Starr 463, Greenberg Division of Cardiology, Weill Medical College of Cornell University, 1300 York Avenue, New York, NY, 10021. Tel: 212-746-6275; Fax: 212-746-7984; gwa2001@med.cornell.edu.

*present address: Clinic for Cardiology and Angiology, Charite University-medicine Berlin 10098 Berlin, Campus Mitte and Experimental and Clinical Research Center, Max Delbrueck Center for Molecular Medicine Berlin, Germany

AUTHOR CONTRIBUTIONS

All authors contributed to design of experiments, data analysis, figure preparation and manuscript writing.
All authors except E.F. and D.J.L. performed experiments.

INTRODUCTION

KCNQ1 is a voltage-gated K^+ channel α subunit noted for its key role in human ventricular repolarization because it generates the I_{Ks} ventricular repolarization current, by co-assembling with the KCNE1 (MinK) single transmembrane domain β subunit1–4. KCNE1 belongs to a family of five genes including KCNE2 (MiRP1), which like KCNE1 can regulate KCNQ1 and other α subunits such as hERG, often endowing unique functional properties5–7. Inherited human gene variants in KCNQ1, hERG, KCNE1 and KCNE2 are all associated with life-threatening cardiac arrhythmias including long QT syndrome3,4,6,8, and may play a role in atrial fibrillation (AF)9–12. These subunits are also expressed in a variety of other tissues, but the possible cardiac effects secondary to their dysfunction in these other tissues are little-studied.

KCNQ1 is unique among the voltage-gated K^+ channel α subunits in that it can form constitutively active, K^+ 'leak' channels; this is achieved by co-assembly with KCNE2 or KCNE3. This permits KCNQ1 to facilitate background K^+ flux in some non-excitable, polarized epithelial cells. Thus, KCNQ1 and KCNE3 are thought to form a channel in the basolateral membrane of colonic crypt cells13. KCNQ1-KCNE2 channels support function of the H^+/K^+-ATPase in the apical membrane of parietal cells; disruption of *Kcnq1* or *Kcne2* in mice causes achlorhydria and gastric hyperplasia14,15.

Analogous to parietal cells and colonic crypt cells in the gastrointestinal tract, thyrocytes are non-excitable, polarized epithelial cells expressing ion transporters essential for the function of the thyroid gland. The thyroid hormones (TH) triiodothyronine (T_3) and tetraiodothyronine (thyroxine, or T_4) are critical for normal growth and development of the fetus and newborn as well as for regulation of metabolism in virtually all tissues at all ages. Because of the scarcity of iodine, an essential constituent of T_3 and T_4, iodide (I^-) deficiency disorders are still prevalent in many areas of the world and are thus at the forefront of global health initiatives. I^- enters thyrocytes via the basolaterally located Na^+/I^- symporter (NIS)16,17 and exits apically into the colloid, where it is covalently incorporated into thyroglobulin, the precursor of T_3 and T_4. NIS-mediated I^- transport uses the downhill Na^+ gradient generated by the Na^+/K^+ ATPase at the basolateral membrane of the thyrocyte. The role of K^+ channels in the thyroid is unknown.

Here, we show that potassium channel subunits KCNQ1 and KCNE2 - originally recognized for their functional roles in repolarizing cardiac myocytes - form a constitutively-active K^+ channel in thyrocytes, and that *Kcne2* is required for normal TH biosynthesis. Aging *Kcne2*$^{-/-}$ mice, and pups from *Kcne2*$^{-/-}$ dams, exhibit a panoply of symptoms including goiter, cardiomegaly, dwarfism and alopecia. Remarkably, these symptoms are alleviated highly efficiently by administration of T_3/T_4 to pups, by supplementing dams with T_4 pre- and postpartum, or by surrogacy with wild-type dams; conversely, symptoms are triggered in wild-type pups by surrogacy with *Kcne2*$^{-/-}$ dams. Put in the context of existing studies, our findings raise the possibility of an endocrine component to some cardiac arrhythmias and early-onset myocardial infarction previously associated with human *KCNQ1* and *KCNE2* genetic variants.

RESULTS

Kcne2$^{-/-}$ pups from Kcne2$^{-/-}$ dams exhibit cardiac hypertrophy, fibrosis and reduced cardiac output

Mutations and polymorphisms in human *KCNQ1* and *KCNE2* are associated with ventricular and atrial cardiac arrhythmias, presumed to arise from dysfunction of the K^+ channels they form in cardiac myocytes4,6,18,19. We previously found that at 3 months of age, *Kcne2*$^{-/-}$ mice from heterozygous crosses have normal echocardiographic parameters and ventricular myocyte size20. In contrast, in the current study, when we bred *Kcne2*$^{-/-}$ pups from homozygous knockout crosses, we found that they exhibited striking cardiomegaly: >2-fold increased heart mass, and >3-fold increased heart weight:bodyweight ratio, at 3 weeks (Fig. 1a). The 3-week-old *Kcne2*$^{-/-}$ pups from *Kcne2*$^{-/-}$ dams also exhibited >50% increases in end-diastolic left ventricular (LV) internal diameter, LV anterior and posterior wall thickness, and a 45% decrease in fractional shortening (Fig. 1b,c). The anterior and posterior wall thickening demonstrate cardiac hypertrophy, and this is probably the primary effect, with the LV dilation and reduced fractional shortening likely arising from a compensatory response (Starling mechanism) to the impaired contractility resulting from sustained hypertrophy.

Ventricular myocytes of 3-week-old *Kcne2*$^{-/-}$ pups from homozygous crosses had a 2-fold larger membrane capacitance than those from age-matched *Kcne2*$^{+/+}$ pups, also indicative of hypertrophy – defined as increased organ or tissue size due to increase in size of the constituent cells (Fig. 1d). Raw amplitudes of two of the predominant mouse ventricular repolarization K^+ currents, $I_{K,slow}$ and $I_{to,f}$, were unaltered by *Kcne2* disruption, but because of the doubling in capacitance this constituted a 2-fold reduction in current density for each. In contrast, the raw amplitude of the steady-state K^+ current (I_{ss}) doubled, indicating that its density did not change with *Kcne2* disruption (Fig. 1d–f).

Hearts from 3-week-old *Kcne2*$^{-/-}$ mice from Kcne2$^{-/-}$ dams (Fig. 1g) also exhibited marked LV fibrosis and papillary muscle degeneration, necrosis and mineralization - a feature of sustained hypertrophy (Fig. 1h). Hepatic fibrosis was also observed, suggesting right heart failure (Fig. 1i) and the liver had an unusually pale appearance (Fig. 1g) possibly indicative of fatty liver. Furthermore, 1-year-old *Kcne2*$^{-/-}$ mice bred from *Kcne2*$^{+/-}$ dams also exhibited cardiomegaly with LV fibrosis (Fig. 1j). In sum, it is apparent that there exists a strong influence of parental genotype on cardiac phenotype of the *Kcne2*$^{-/-}$ offspring, and also that aging *Kcne2*$^{-/-}$ mice from heterozygous parents show severe cardiovascular hypertrophy and fibrosis not yet manifested in their 3-month-old counterparts20.

Kcne2$^{-/-}$ mice exhibit dwarfism and alopecia

Aside from their cardiac pathology, *Kcne2*$^{-/-}$ mice exhibited other gross abnormalities that were exacerbated by the maternal *Kcne2*$^{-/-}$ genotype. Pups from *Kcne2*$^{-/-}$ dams exhibited 50% embryonic lethality whether the sire was *Kcne2*$^{-/-}$ or *Kcne2*$^{+/-}$ (Fig. 2a). Maternal genotype was the determining factor in litter size: litters from *Kcne2*$^{+/-}$ dams with *Kcne2*$^{-/-}$ sires were of normal size, and surviving pups in litters from *Kcne2*$^{-/-}$ × *Kcne2*$^{+/-}$ crosses showed an approximately Mendelian distribution (Fig. 2a). *Kcne2*$^{-/-}$ pups from *Kcne2*$^{-/-}$

dams also exhibited severe dwarfism (Fig. 2b,c). While birth weights were similar in all cases, mean body weight of pups from *Kcne2*$^{-/-}$ × *Kcne2*$^{-/-}$ crosses was 40% lower than that of pups from *Kcne2*$^{+/+}$ × *Kcne2*$^{-/-}$ crosses at 5 weeks. Reduced body mass correlated with the maternal *Kcne2*$^{-/-}$ genotype, but also to pup genotype since pups from (+/−) sires were significantly larger than those from *Kcne2*$^{-/-}$ sires (both with *Kcne2*$^{-/-}$ dams) (Fig. 2d). By 15 weeks of age mean bodyweights were similar regardless of pup genotype (Supplementary Fig. 1a).

Radiological examination revealed retarded skeletal development in the *Kcne2*$^{-/-}$ pups, producing dwarfism due to slow growth of both long bones and vertebrae. This was also apparent in the form of larger epiphyseal gaps and less ossification of the epiphyses in the large joints, which were irregularly shaped, fragmented, and heterogeneously sclerotic, characteristic of slow multifocal ossification (Fig. 2c).

Surprisingly, *Kcne2*$^{-/-}$ pups from homozygous crosses also exhibited striking alopecia of the trunk which began at 1–2 weeks of age and peaked at 4–5 weeks (Fig. 2b,e–g). Alopecia was also observed in aging *Kcne2*$^{-/-}$ mice from *Kcne2*$^{+/-}$ × *Kcne2*$^{+/-}$ crosses, initiating between the ears then spreading postero-dorsally with an abrupt loss of mature hair follicles at the transition zones (Fig. 2h–j).

Cardiomegaly, dwarfism and alopecia in Kcne2$^{-/-}$ mice are attenuated by wild-type surrogacy, T_4 supplementation of dams, or T_3/T_4 administration to pups

Considering the combination of cardiac hypertrophy, cardiac and hepatic fibrosis, dwarfism, alopecia, and skeletal abnormalities indicative of retarded development, we investigated whether or not hypothyroidism might be the underlying cause. To test this hypothesis, we first determined serum TH concentrations. Indeed, serum T_4 was 2-fold decreased, and TSH 2-fold increased, in 3-week-old *Kcne2*$^{-/-}$ pups from homozygous crosses compared to *Kcne2*$^{+/+}$ pups from homozygous crosses (Fig. 3a), confirming the former were hypothyroid. Serum T_4 and TSH were, however, normal in nubile 3–6 month old *Kcne2*$^{-/-}$ mice from heterozygous crosses (Supplementary Fig. 2), consistent with growth, litter size, and cardiac morphology trends (see Fig. 2 and 20). By age 12–15 months T_4 and TSH were trending down and up respectively in mice from heterozygous crosses (Supplementary Fig. 2), consistent with a latent hypothyroidism, and the late onset of alopecia (Fig. 2h), cardiac hypertrophy and fibrosis (Fig. 1j). Thyroid glands from these aged mice bred from *Kcne2*$^{+/-}$ crosses showed a 40% greater mean mass post-mortem than *Kcne2*$^{+/+}$ thyroids, with *Kcne2*$^{+/-}$ thyroids having intermediate mean mass, indicative of goiter formation due to *Kcne2* disruption (Fig. 3 b). In contrast to nubile adult mice, pregnant *Kcne2*$^{-/-}$ dams exhibited almost 3-fold reduced serum T_4 concentration compared to pregnant *Kcne2*$^{+/+}$ dams (Figure 3 c), suggesting an explanation for the exaggerated phenotype and reduced litter size of *Kcne2*$^{-/-}$ pups bred from *Kcne2*$^{-/-}$ dams (Fig. 2). Consistent with previous reports for mice and rats (but in contrast to humans)21,22, pregnant mice in our study exhibited lower serum T_4 than age- and genotyped-matched nubile adults (Fig. 3c; Supplementary Fig. 2).

We next tested whether or not surrogacy of pre-weaning pups would alleviate any of the observed abnormalities. Significantly, normal body weight was fully restored in *Kcne2*$^{-/-}$

pups from *Kcne2*$^{-/-}$ × *Kcne2*$^{-/-}$ crosses by pre-weaning surrogacy with *Kcne2*$^{+/+}$ dams (Fig. 3d,e). Conversely, pre-weaning surrogacy of *Kcne2*$^{+/+}$ pups with *Kcne2*$^{-/-}$ dams resulted in mean pre-weaning body weight similar to *Kcne2*$^{-/-}$ pups, and intermediate body weight in post-weaning pups (Fig. 3d,e). These data suggested the possibility that maternal TH passed through milk – perhaps at higher concentrations, or in higher volumes of milk, from wild-type dams – were compensating for the defect in pups. Confirming the role of TH in body weight differences, *Kcne2*$^{-/-}$ pups born and raised by *Kcne2*$^{-/-}$ dams and from *Kcne2*$^{-/-}$ sires, showed significantly improved body weight by 3 weeks of age after T_3/T_4 administration every 48 hours (QOD) from birth (Fig. 3e, Supplementary Fig. 1b). Furthermore, T_4 supplementation of *Kcne2*$^{-/-}$ dams, from 2 weeks pre-birth to weaning, also resulted in normal pup body weight (Fig. 3e).

Dermatologic disorders occur frequently in hypothyroidism23. Remarkably, here we found that alopecia was completely reversed in adult *Kcne2*$^{-/-}$ mice with 2 weeks QOD administration of T_3/T_4 (exemplars in Fig. 3f,g). Alopecia was also completely reversed in 19 of 21 *Kcne2*$^{-/-}$ pups by 10 days QOD T_3/T_4 administration, in 19/20 *Kcne2*$^{-/-}$ pups by surrogacy with *Kcne2*$^{+/+}$ dams, and in 16/16 *Kcne2*$^{-/-}$ pups by T_4 supplementation of their mothers from 2 weeks pre-birth to weaning. Conversely, alopecia was observed in 13/23 *Kcne2*$^{+/+}$ pups surrogated with *Kcne2*$^{-/-}$ dams (Fig. 3g).

Hypothyroidism is associated with dilated and hypertrophic cardiomyopathies, reduced fractional shortening and heart failure24. Supporting a link between these cardiac defects and the hypothyroidism observed in *Kcne2*$^{-/-}$ mice, surrogacy with *Kcne2*$^{+/+}$ dams resulted in a dramatic reduction in the relative mass of the heart compared to body weight; conversely, surrogacy of *Kcne2*$^{+/+}$ pups with *Kcne2*$^{-/-}$ dams had the opposite effect (Fig. 3 h,i). As observed with non-surrogated *Kcne2*$^{-/-}$ pups (Fig. 1g), the liver of *Kcne2*$^{+/+}$ pups surrogated with *Kcne2*$^{-/-}$ dams had an unusually pale appearance possibly indicative of fatty liver (Fig. 3h). Furthermore, echocardiographic determination of the potential beneficial effects of surrogacy of *Kcne2*$^{-/-}$ pups with *Kcne2*$^{+/+}$ dams showed significant reduction in ventricular wall thickness and chamber diameter, and increased fractional shortening compared to non-surrogated *Kcne2*$^{-/-}$ pups (Fig. 3j).

KCNE2 and KCNQ1 form a TSH-stimulated thyrocyte K^+ channel

Our data (Fig. 1–Fig. 3) suggested a potential role for KCNE2 in TH biosynthesis. Previous studies indicate that KCNE2 probably forms channel complexes with the KCNQ1 K^+ channel α subunit in gastric epithelium14,15,25,26. Here, we found that both KCNE2 and KCNQ1 are expressed in human (Fig. 4a) and mouse (Fig. 4b–d) thyroid glands; in both species they partially co-localized with NIS, the basolateral membrane glycoprotein that mediates active I^- transport, the first step in TH biosynthesis. Furthermore, thyroid follicular epithelia in *Kcne2*$^{-/-}$ mice exhibited abnormal architecture: compared to those in *Kcne2*$^{+/+}$ mice, *Kcne2*$^{-/-}$ thyrocytes were often flattened and less abundant (Fig. 4e,f).

We next sought to determine whether KCNQ1-KCNE2 K^+ currents were expressed in thyrocytes, employing the highly functional rat thyroid-derived FRTL5 cell line. We detected endogenously-expressed KCNQ1 and KCNE2 proteins, which appeared to be upregulated by TSH or its major downstream effector, cAMP, in FRTL5 cell membrane

fractions (Fig. 4g). We then measured endogenous currents from FRTL5 cells using patch-clamp recording in the whole-cell configuration. A TSH-stimulated K^+ current in FRTL5 cells bore the signature linear current-voltage relationship of KCNQ1-KCNE2 channels and was inhibited by the KCNQ-specific antagonist XE991 (Fig. 4h,i). In sum, KCNQ1-KCNE2 channels are expressed in human and rodent thyrocytes, where they generate a TSH-stimulated, constitutively-active K^+ current.

KCNE2 is required for normal thyroid I^- accumulation

TH requirements are especially high in early development: developing fetuses and neonates rely upon not only their own TH biosynthesis, but also maternal T_4 *in utero* and perhaps *via* milk. Therefore, we examined thyroid I^- accumulation, a critical step in TH biosynthesis, in lactating dams and their pups. We injected ^{124}I only into the tail vein of lactating dams, which were then placed back together with their pups to feed them. Both dams and pups were imaged by positron emission tomography (PET). *Kcne2*$^{-/-}$ dams showed a striking defect in ^{124}I accumulation in the thyroid, with 4-fold less accumulation over the first hour post-injection and continuing deficiency in the following three days (Fig. 5a–c). In pups, whose sole source of ^{124}I was dams' milk, *Kcne2* deletion caused a 5-fold reduction of pup thyroid ^{124}I accumulation 24-hours post-injection of dams, and continuing deficiency for the following 2 days (Fig. 5d,e). When normalized to stomach ^{124}I count the thyroid ^{124}I count was reduced 8-fold in *Kcne2*$^{-/-}$ pups compared to wild-type pups at 72 hours post-injection of the dam (Fig. 5f).

Thus, *Kcne2* deletion causes a thyroid I^- accumulation defect, which in turn causes a TH biosynthesis defect, the gross phenotypic effects of which are particularly striking in pre-weaning pups feeding from *Kcne2*$^{-/-}$ dams. To examine the mechanistic basis for this, and for the beneficial effects of surrogacy by *Kcne2*$^{+/+}$ dams, we first performed PET on pups surrogated with dams of opposite genotype, after tail vein injection of lactating dams with ^{124}I followed by imaging of pups feeding from them. Strikingly, we found that *Kcne2*$^{-/-}$ pups feeding from *Kcne2*$^{+/+}$ dams had higher stomach and thyroid ^{124}I counts (measured as peak counts/cc), and higher thyroid:stomach count ratio, than *Kcne2*$^{+/+}$ pups feeding from *Kcne2*$^{-/-}$ dams (Fig. 6a–c). This suggested that the surrogating dams' genotype was critical in determining thyroid ^{124}I uptake of pups, although pup genotype was also important because when pups of either genotype fed from *Kcne2*$^{+/+}$ dams, *Kcne2*$^{+/+}$ pups still had an almost 2-fold higher thyroid:stomach count ratio at 48–72 hrs compared to *Kcne2*$^{-/-}$ pups (Fig. 5f, Fig. 6c).

Total thyroid and total body activity was also quantified for all surrogated and non-surrogated pups, thereby permitting comparison of thyroid radioactive iodide uptake (RAIU) as a percentage of whole body activity (Fig. 6d). Total thyroid ^{124}I was higher in all pups when feeding from *Kcne2*$^{+/+}$ dams than when feeding from *Kcne2*$^{-/-}$ dams, whereas total body ^{124}I was only significantly higher than other groups for *Kcne2*$^{-/-}$ pups feeding from *Kcne2*$^{+/+}$ dams (Fig. 6d *left*). In contrast, thyroid RAIU – a measure of the efficiency of the thyroid at accumulating ^{124}I from the available total body ^{124}I – was only significantly higher than other groups in *Kcne2*$^{+/+}$ pups feeding from *Kcne2*$^{+/+}$ dams (Fig. 6d *right*). These data again demonstrated that *Kcne2*$^{-/-}$ pups' thyroids are less efficient than those of

Kcne2$^{+/+}$ pups at accumulating I^-, but also indicated that *Kcne2*$^{-/-}$ dams supply less I^- to their pups than do *Kcne2*$^{+/+}$ dams. These results also revealed that *Kcne2*$^{-/-}$ pups are relatively better at accumulating total body I^- than *Kcne2*$^{+/+}$ pups.

Examining first the poor delivery of I^- from *Kcne2*$^{-/-}$ dams, we compared milk ejection from *Kcne2*$^{+/+}$ and *Kcne2*$^{-/-}$ dams by weighing pups before and after feeding, as previously described27. This led to the discovery that *Kcne2*$^{-/-}$ dams have a highly significant milk ejection defect, manifested as pups (of either genotype) failing to gain weight (from milk ingestion) during the first 30 min of feeding from *Kcne2*$^{-/-}$ dams, in sharp contrast to pups feeding from *Kcne2*$^{+/+}$ dams (Fig. 6e). Similar results were seen over the first 60 min of feeding (Supplementary Fig. 3). Importantly, *Kcne2*$^{+/+}$ and *Kcne2*$^{-/-}$ pups showed no significant difference in their feeding rate measured by weight gain (Fig. 6e, Supplementary Fig. 3). Pups were latched on to dams of either genotype for the entire period under study (30 or 60 min). Thus, the milk ejection defects were not related to behavioral differences in either pups or dams, and instead reflected a pathophysiological defect in milk ejection by *Kcne2*$^{-/-}$ dams. Hypothyroid rats were previously shown to have impaired milk ejection due to reduced serum oxytocin compared to euthyroid rats27. Accordingly, here we found that injection of *Kcne2*$^{-/-}$ dams with oxytocin returned their milk ejection to the same level as *Kcne2*$^{+/+}$ dams (Fig. 6e). The milk ejection defect was probably a dominant factor in the beneficial effects of *Kcne2*$^{+/+}$ surrogacy, and the negative effects of *Kcne2*$^{-/-}$ surrogacy. Additionally, however, we discovered that milk from *Kcne2*$^{-/-}$ dams contained only half as much T_4 as that from *Kcne2*$^{+/+}$ dams (Fig. 6f), potentially also contributing to the observed effects of surrogacy.

Finally, addressing the superior total body accumulation of I^- by *Kcne2*$^{-/-}$ pups, we found equal serum I^- concentrations in non-surrogated 3-week-old *Kcne2*$^{+/+}$ and *Kcne2*$^{-/-}$ pups (Fig. 6g), suggesting that despite inferior milk ejection by *Kcne2*$^{-/-}$ dams, *Kcne2*$^{-/-}$ pups were able to maintain normal plasma I^- concentrations. This was not surprising given that hypothyroidism is known to result in decreased I^- excretion28.

DISCUSSION

More than a decade ago, KCNQ1 mRNA was found to be expressed at a higher level in human thyroid than in the heart or stomach29, but its role in the thyroid has not previously been reported. Furthermore, *kcnq1* gene-disrupted mice were previously found, like our *Kcne2*$^{-/-}$ mice, to have enlarged hearts and thickened ventricular walls, but the mechanistic basis for this was not described30,31.

T_3 and T_4 biosynthesis requires active I^- transport in the thyroid, where I^- concentrations reach 20–40 times that of the plasma. NIS, located on the basolateral side of the thyrocytes – thyroid epithelial cells which encircle the colloid – transports I^- into the thyrocyte; at the cell/colloid interface I^- ion is oxidized and covalently incorporated into thyroglobulin, for TH production17. NIS function requires a basolateral Na^+/K^+-ATPase for Na^+ efflux but the necessity for other channels or transporters in this process is not known. Here, KCNQ1-KCNE2 is identified as a TSH-stimulated thyrocyte K^+ channel critical for normal thyroid I^- accumulation, and probably expressed predominantly at the basolateral membrane.

The dramatic effects of surrogacy in the current study add to the debate over whether or not maternal T_4 is at high enough concentrations in milk to deliver therapeutic effects in hypothyroxinaemic newborns32. Our findings suggest mouse milk TH could be beneficial in this context, as there are significant levels of T_4 in milk, reduced by *Kcne2* disruption (Fig. 6f), albeit the poor development of pups feeding from *Kcne2*$^{-/-}$ dams probably arises from a combination of this and the impaired milk ejection of *Kcne2*$^{-/-}$ dams (Fig. 6e). The mechanisms underlying the whole-animal and molecular effects of surrogacy appear complex, as one would expect. We speculate that the thyroid I^- accumulation of *Kcne2*$^{-/-}$ pups is diminished by *Kcne2* deletion but that this is partially balanced by e.g., adaptation to developing in a low maternal T_4 environment in the womb (Fig. 3c) and being initially fed with poorly-ejected, low-T_4 milk (Fig. 6e,f). The end result is that *Kcne2*$^{-/-}$ pups are less efficient at accumulating thyroid I^- compared to *Kcne2*$^{+/+}$ pups when either are fed by *Kcne2*$^{+/+}$ dams, but when fed by *Kcne2*$^{-/-}$ dams their thyroid RAIUs are similar (Fig. 6d). Part of this adaptation may involve reduced I^- excretion by *Kcne2*$^{-/-}$ pups, as previously reported28 and supported by our current data (Fig. 6d,e,g). Interestingly, as observed for NIS16,33, KCNQ1 is also expressed in mammary gland epithelium, where it may co-assemble with KCNE3 to play a role in K^+ homeostasis34. While a role for KCNE2 in mammary epithelial function should not be ruled out, our PET data demonstrate that mammary gland I^- uptake is not impaired in *Kcne2*$^{-/-}$ dams (Fig. 5). Nevertheless, the phenotypes we describe herein for *Kcne2*$^{-/-}$ pups bred from homozygous *Kcne2*$^{-/-}$ crosses include features such as alopecia and cardiac hypertrophy, not always observed in hypothyroid mouse models35. While this may at least partly be explained by the combination of both *Kcne2*$^{-/-}$ dam and pup (heterozygous crosses are typically employed), it could possibly indicate additional pathogenesis beyond thyroid impairment but successfully treatable by TH supplementation.

Human thyroid dysfunction negatively impacts the brain, heart and GI tract; fatalities may occur from thyroid storm in hyperthyroidism, and myxedema coma in hypothyroidism36. In addition, thyroid dysfunction during pregnancy increases the risk of adverse maternal and fetal outcomes37–39. Subclinical human maternal hypothyroxinemia causes severe neurodevelopmental disorders40, may include changes in blood lipid profile, myocardial function, and neuropsychiatric function41–43, and is an independent risk factor in heart failure due to structural and electrical remodeling in the heart24. Importantly, a SNP near *KCNE2* was recently shown to associate with early-onset myocardial infarction44 – suggesting the possibility of a genetic link to previously-reported subclinical hypothyroidism-associated accelerated coronary artery disease and myocardial infarction45.

Subclinical hypothyroidism is also associated with prolonged QTc46, a hallmark of loss-off-function mutations in *KCNE2* and *KCNQ1*3,6, and with AF, an increasingly prevalent disease in the aging population47,48 that is also associated with some *KCNQ1* and *KCNE2* gene variants 9,12. As many as 13% of patients with idiopathic AF exhibit biochemical evidence of hyperthyroidism49; in one study, 62% of 163 patients reverted to sinus rhythm within 8–10 weeks after treatment for hyperthyroidism returned them to a euthyroid state50. Therefore, the finding here that KCNE2-KCNQ1 channels contribute to thyroid function raises the tantalizing hypothesis that there is a thyroid component to some *KCNE2*- or

KCNQ1-associated cardiac arrhythmias. In previous studies of sudden cardiac or unexplained death, it was often assumed that ion channel gene mutations were not causative in those cases exhibiting overt structural heart disease upon autopsy51; historically, 'electrical' heart diseases arising from ion channel defects have mostly been considered genetically distinct from 'structural' heart disease, although variants in the human SCN5A Na^+ channel gene have been associated with dilated cardiomyopathy52. Our current findings suggest reconsideration of patients with structural heart disease exhibiting ventricular or atrial arrhythmias, given the possibility that mutations in *KCNQ1* and *KCNE2* could be arrhythmogenic due both to primary electrical defects in myocyte K^+ channels containing these subunits, and to cardiac structural abnormalities arising secondarily from thyroid dysfunction due to defective thyroid KCNQ1-KCNE2 channels.

Identification of KCNE2-KCNQ1 as a thyrocyte channel important for I^- accumulation may also have therapeutic implications. Agonists and antagonists of KCNQ1-KCNE2 channels have already been developed. Because the pharmacology of KCNQ1-KCNE2 complexes is markedly different from that of homomeric KCNQ1, KCNQ1-KCNE1, or KCNQ1-KCNE3 channels53, identification of the requirement of KCNQ1-KCNE2 complexes for normal thyroid function may permit semi-specific, reversible pharmacological targeting of the KCNQ1-KCNE2 complex to treat thyroid disease.

Supplementary Material

Refer to Web version on PubMed Central for supplementary material.

ACKNOWLEDGEMENTS

G.W.A. is supported by the US National Heart, Lung and Blood Institute (HL079275) and the American Heart Association (0855756D). N.C. is supported by the US National Institute of Diabetes and Digestive and Kidney Diseases (DK41544) and the US National Cancer Institute (CA098390). M.P. is supported by US National Institutes of Health Medical Scientist Training Grant 5T32GM002788. We are grateful for expert technical assistance from S. Backovic, L. Cohen-Gould, G. J.-S. Abbott, K. La Perle, the Molecular Cytology Core Facility of Memorial Sloan-Kettering Cancer Center, and C. Basson and J. Chen (WCMC Center for Molecular Cardiology Small Animal Physiology Core Facility). We also thank T. Denecke for interpreting the radiographs and B. Abbott for critical reading of the manuscript.

ABBREVIATIONS

AF	atrial fibrillation
AW	anterior wall
cAMP	cyclic AMP
FS	fractional shortening
IVST	interventricular septal thickness
ESD	end-systolic dimension
EDD	end-diastolic dimension
LV	left ventricular

MiRP	MinK-related peptide
NIS	Na^+/I^- symporter
PET	positron emission tomography
PW	posterior wall
T3	triiodothyronine
T4	tetraiodothyronine/thyroxine
TH	thyroid hormone(s)
TSH	thyroid-stimulating hormone.

REFERENCES

1. Barhanin J, et al. K(V)LQT1 and lsK (minK) proteins associate to form the I(Ks) cardiac potassium current. Nature. 1996; 384:78–80. [PubMed: 8900282]
2. Sanguinetti MC, et al. Coassembly of K(V)LQT1 and minK (IsK) proteins to form cardiac I(Ks) potassium channel. Nature. 1996; 384:80–83. [PubMed: 8900283]
3. Splawski I, Tristani-Firouzi M, Lehmann MH, Sanguinetti MC, Keating MT. Mutations in the hminK gene cause long QT syndrome and suppress IKs function. Nat Genet. 1997; 17:338–340. [PubMed: 9354802]
4. Tyson J, et al. IsK and KvLQT1: mutation in either of the two subunits of the slow component of the delayed rectifier potassium channel can cause Jervell and Lange-Nielsen syndrome. Hum Mol Genet. 1997; 6:2179–2185. [PubMed: 9328483]
5. McDonald TV, et al. A minK-HERG complex regulates the cardiac potassium current I(Kr). Nature. 1997; 388:289–292. [PubMed: 9230439]
6. Abbott GW, et al. MiRP1 Forms IKr Potassium Channels with HERG and Is Associated with Cardiac Arrhythmia. Cell. 1999; 97:175–187. [PubMed: 10219239]
7. McCrossan ZA, Abbott GW. The MinK-Related Peptides. Neuropharmacology. 2004; 47:787–821. [PubMed: 15527815]
8. Curran ME, et al. A molecular basis for cardiac arrhythmia: HERG mutations cause long QT syndrome. Cell. 1995; 80:795–803. [PubMed: 7889573]
9. Chen YH, et al. KCNQ1 gain-of-function mutation in familial atrial fibrillation. Science. 2003; 299:251–254. [PubMed: 12522251]
10. Ehrlich JR, Zicha S, Coutu P, Hebert TE, Nattel S. Atrial fibrillation-associated minK38G/S polymorphism modulates delayed rectifier current and membrane localization. Cardiovasc Res. 2005; 67:520–528. [PubMed: 16039273]
11. Temple J, et al. Atrial Fibrillation in KCNE1-Null Mice. Circ Res. 2005; 97:62–69. [PubMed: 15947250]
12. Yang Y, et al. Identification of a KCNE2 gain-of-function mutation in patients with familial atrial fibrillation. Am J Hum Genet. 2004; 75:899–905. [PubMed: 15368194]
13. Schroeder BC, et al. A constitutively open potassium channel formed by KCNQ1 and KCNE3. Nature. 2000; 403:196–199. [PubMed: 10646604]
14. Lee MP, et al. Targeted disruption of the Kvlqt1 gene causes deafness and gastric hyperplasia in mice. J Clin Invest. 2000; 106:1447–1455. [PubMed: 11120752]
15. Roepke TK, et al. The KCNE2 potassium channel ancillary subunit is essential for gastric acid secretion. J Biol Chem. 2006; 281:23740–23747. [PubMed: 16754665]
16. Dai G, Levy O, Carrasco N. Cloning and characterization of the thyroid iodide transporter. Nature. 1996; 379:458–460. [PubMed: 8559252]

17. Dohan O, et al. The sodium/iodide Symporter (NIS): characterization, regulation, and medical significance. Endocr Rev. 2003; 24:48–77. [PubMed: 12588808]
18. Sesti F, et al. A common polymorphism associated with antibiotic-induced cardiac arrhythmia. Proc Natl Acad Sci U S A. 2000; 97:10613–10618. [PubMed: 10984545]
19. Splawski I, Timothy KW, Vincent GM, Atkinson DL, Keating MT. Molecular basis of the long-QT syndrome associated with deafness. N Engl J Med. 1997; 336:1562–1567. [PubMed: 9164812]
20. Roepke TK, et al. Targeted deletion of kcne2 impairs ventricular repolarization via disruption of I(K,slow1) and I(to,f). Faseb J. 2008; 22:3648–3660. [PubMed: 18603586]
21. Fukuda H, Ohshima K, Mori M, Kobayashi I, Greer MA. Sequential changes in the pituitary-thyroid axis during pregnancy and lactation in the rat. Endocrinology. 1980; 107:1711–1716. [PubMed: 7428688]
22. Imaizumi M, et al. Pregnancy and murine thyroiditis: thyroglobulin immunization leads to fetal loss in specific allogeneic pregnancies. Endocrinology. 2001; 142:823–829. [PubMed: 11159855]
23. Burman KD, McKinley-Grant L. Dermatologic aspects of thyroid disease. Clin Dermatol. 2006; 24:247–255. [PubMed: 16828405]
24. Tang YD, et al. Low thyroid function leads to cardiac atrophy with chamber dilatation, impaired myocardial blood flow, loss of arterioles, and severe systolic dysfunction. Circulation. 2005; 112:3122–3130. [PubMed: 16275864]
25. Dedek K, Waldegger S. Colocalization of KCNQ1/KCNE channel subunits in the mouse gastrointestinal tract. Pflugers Arch. 2001; 442:896–902. [PubMed: 11680623]
26. Grahammer F, et al. The cardiac K+ channel KCNQ1 is essential for gastric acid secretion. Gastroenterology. 2001; 120:1363–1371. [PubMed: 11313306]
27. Hapon MB, Simoncini M, Via G, Jahn GA. Effect of hypothyroidism on hormone profiles in virgin, pregnant and lactating rats, and on lactation. Reproduction. 2003; 126:371–382. [PubMed: 12968945]
28. Oddie TH, Meade JH Jr, Myhill J, Fisher DA. Dependence of renal clearance of radioiodide on sex, age and thyroidal status. J Clin Endocrinol Metab. 1966:1293–1296. [PubMed: 5959522]
29. Yang WP, et al. KvLQT1, a voltage-gated potassium channel responsible for human cardiac arrhythmias. Proc Natl Acad Sci U S A. 1997; 94:4017–4021. [PubMed: 9108097]
30. Casimiro MC, et al. Targeted disruption of the Kcnq1 gene produces a mouse model of Jervell and Lange-Nielsen Syndrome. Proc Natl Acad Sci U S A. 2001; 98:2526–2531. [PubMed: 11226272]
31. Elso CM, et al. Heightened susceptibility to chronic gastritis, hyperplasia and metaplasia in Kcnq1 mutant mice. Hum Mol Genet. 2004; 13:2813–2821. [PubMed: 15385447]
32. van Wassenaer AG, et al. The quantity of thyroid hormone in human milk is too low to influence plasma thyroid hormone levels in the very preterm infant. Clin Endocrinol (Oxf). 2002; 56:621–627. [PubMed: 12030913]
33. Tazebay UH, et al. The mammary gland iodide transporter is expressed during lactation and in breast cancer. Nat Med. 2000; 6:871–878. [PubMed: 10932223]
34. Vantol B, et al. Contribution of KCNQ1 to the regulatory volume decrease in the human mammary epithelial cell line, MCF-7. Am J Physiol Cell Physiol. 2007; 293:C1010–C1019. [PubMed: 17596298]
35. Gruters A, Krude H, Biebermann H. Molecular genetic defects in congenital hypothyroidism. Eur J Endocrinol. 2004; 151(Suppl 3):U39–U44. [PubMed: 15554885]
36. Gavin LA. Thyroid crises. Med Clin North Am. 1991; 75:179–193. [PubMed: 1987442]
37. Kasatkina EP, et al. Gestational hypothyroxinemia and cognitive function in offspring. Neurosci Behav Physiol. 2006; 36:619–624. [PubMed: 16783515]
38. Palagiano A. Immunological abortion: the thyroid factor. Minerva Ginecol. 2006; 58:471–477. [PubMed: 17108877]
39. Song L, McGee JA, Walsh EJ. Consequences of combined maternal, fetal and persistent postnatal hypothyroidism on the development of auditory function in Tshrhyt mutant mice. Brain Res. 2006; 1101:59–72. [PubMed: 16780814]
40. Opazo M, et al. Maternal hypothyroxinemia impairs spatial learning and synaptic nature and function in the offspring. Endocrinology. 2008; 149:5097–5106. [PubMed: 18566112]

41. Pallas D, et al. Increased mean serum thyrotropin in apparently euthyroid hypercholesterolemic patients: does it mean occult hypothyroidism? J Endocrinol Invest. 1991; 14:743–746. [PubMed: 1761809]
42. Haggerty JJ Jr, et al. Subclinical hypothyroidism: a review of neuropsychiatric aspects. Int J Psychiatry Med. 1990; 20:193–208. [PubMed: 2203696]
43. Glueck CJ, Lang J, Tracy T, Speirs J. The common finding of covert hypothyroidism at initial clinical evaluation for hyperlipoproteinemia. Clin Chim Acta. 1991; 201:113–122. [PubMed: 1790615]
44. Kathiresan S, et al. Genome-wide association of early-onset myocardial infarction with single nucleotide polymorphisms and copy number variants. Nat Genet. 2009; 41:334–341. [PubMed: 19198609]
45. Hak AE, et al. Subclinical hypothyroidism is an independent risk factor for atherosclerosis and myocardial infarction in elderly women: the Rotterdam Study. Ann Intern Med. 2000; 132:270–278. [PubMed: 10681281]
46. Bakiner O, et al. Subclinical hypothyroidism is characterized by increased QT interval dispersion among women. Med Princ Pract. 2008; 17:390–394. [PubMed: 18685279]
47. Sawin CT, et al. Low serum thyrotropin concentrations as a risk factor for atrial fibrillation in older persons. N Engl J Med. 1994; 331:1249–1252. [PubMed: 7935681]
48. Levy S. Epidemiology and classification of atrial fibrillation. J Cardiovasc Electrophysiol. 1998; 9:S78–S82. [PubMed: 9727680]
49. Forfar JC, Miller HC, Toft AD. Occult thyrotoxicosis: a correctable cause of "idiopathic" atrial fibrillation. Am J Cardiol. 1979; 44:9–12. [PubMed: 110126]
50. Nakazawa HK, Sakurai K, Hamada N, Momotani N, Ito K. Management of atrial fibrillation in the post-thyrotoxic state. Am J Med. 1982; 72:903–906. [PubMed: 7091161]
51. Tester DJ, Ackerman MJ. Postmortem long QT syndrome genetic testing for sudden unexplained death in the young. J Am Coll Cardiol. 2007; 49:240–246. [PubMed: 17222736]
52. Olson TM, et al. Sodium channel mutations and susceptibility to heart failure and atrial fibrillation. Jama. 2005; 293:447–454. [PubMed: 15671429]
53. Heitzmann D, et al. Heteromeric KCNE2/KCNQ1 potassium channels in the luminal membrane of gastric parietal cells. J Physiol. 2004; 561:547–557. [PubMed: 15579540]

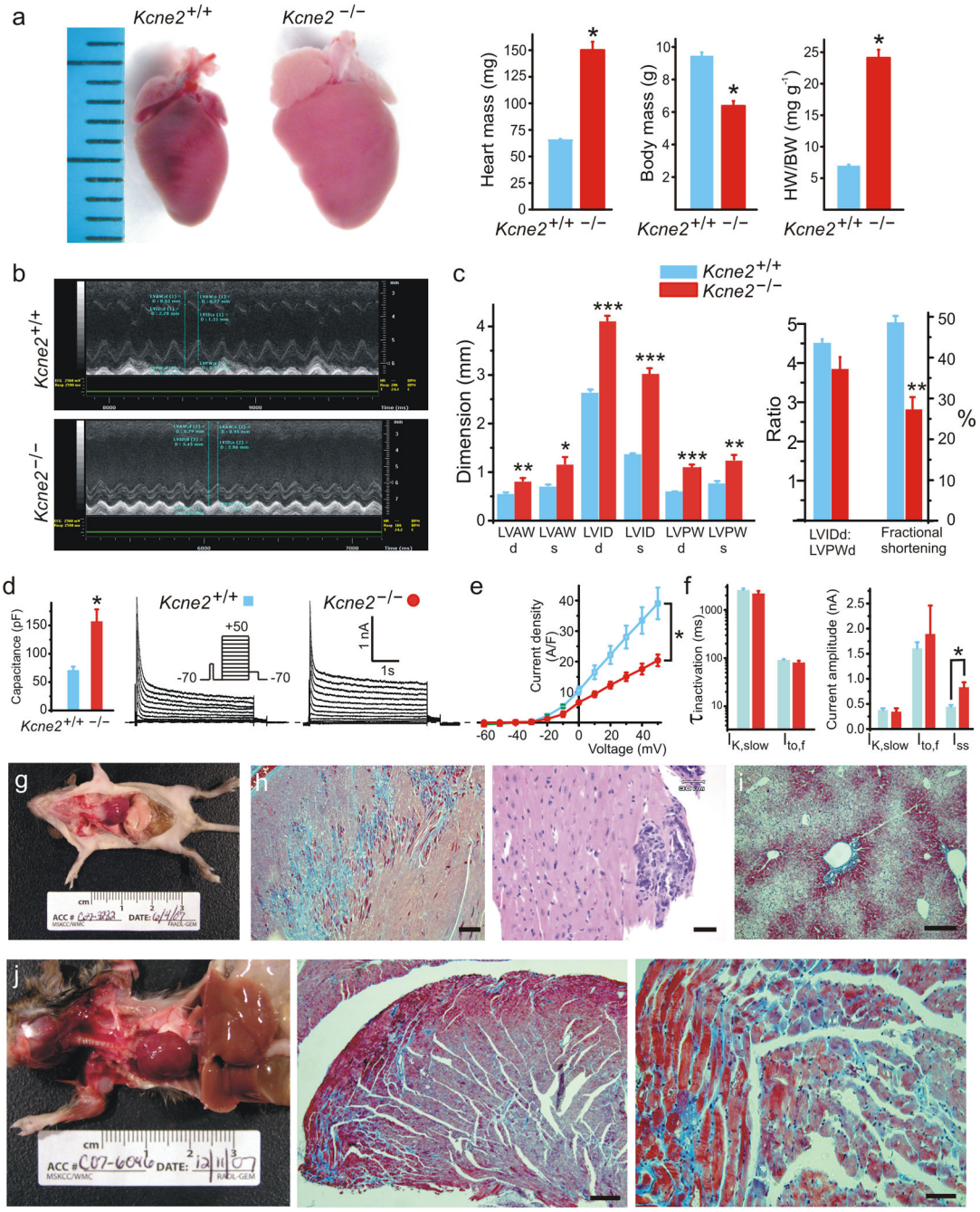

Figure 1. *Kcne2* disruption causes cardiac hypertrophy, fibrosis and reduced fractional shortening

(**a**) *Left*, external view of exemplar hearts from 3-week-old *Kcne2*$^{+/+}$ (*left*) and *Kcne2*$^{-/-}$ (*right*) mice from homozygous crosses. *Right*, mean heart mass, body mass, and heart weight/bodyweight (HW/BW; mg g^{-1}) for mice as in panel a (n = 9–14).* $P < 0.000001$. (**b**)Exemplar transthoracic echocardiograms for a 3-week-old *Kcne2*$^{+/+}$ pup from a *Kcne2*$^{+/+}$ dam and a *Kcne2*$^{-/-}$ pup from a *Kcne2*$^{-/-}$ dam.

(**c**) Mean echocardiographic parameters from recordings as in panel b. d/s, diastolic/systolic; LVAW, left ventricular anterior wall thickness; LVID, left ventricular internal diameter; LVPW, left ventricular posterior wall thickness, $n = 4$ per group. * $P < 0.05$; ** $P < 0.005$; *** $P < 0.0005$, by one-way ANOVA.

(**d**) *Left*, mean cell capacitance for ventricular myocytes isolated from 3-week-old pups from homozygous crosses, $n = 6–8$; *$P < 0.001$. *Right*, exemplar whole-cell recordings from ventricular myocytes as in *left*. Insets: voltage protocol and scale bars.

(**e**) Mean peak current densities for *Kcne2*$^{+/+}$ (blue) and *Kcne2*$^{-/-}$ (red) myocytes as in panel d, $n = 6–8$; *$P < 0.05$.

(**f**) *Left*, current inactivation τ values for *Kcne2*$^{+/+}$ (blue) versus *Kcne2*$^{-/-}$ (red) myocytes as in panel e. *Right*, current amplitudes from double exponential fits for *Kcne2*$^{+/+}$ (solid) versus *Kcne2*$^{-/-}$ (open) myocytes as in panel g. *$P < 0.001$. Current decay was best fit with two exponentials with parameters resembling $I_{to,f}$ and $I_{K,slow}$, and a steady-state current, I_{ss}.

(**g–i**) Cardiac tissue from 3-week-old *Kcne2*$^{-/-}$ mice bred from *Kcne2*$^{-/-}$ dams.

(**g**) Exemplar necropsy.

(**h**) *Left*, exemplar Masson's trichrome-stained left ventricle showing collagen (*blue*) indicative of fibrosis. Scale bar, 150 μm. *Right*, exemplar H&E-stained papillary muscle. Scale bar, 30 μm.

(**i**) Exemplar Masson's trichrome stained liver showing marked perisinusoidal fibrosis (*blue*). Scale bar, 200 μm.

(**j**) Cardiac tissue from 15-month-old *Kcne2*$^{-/-}$ mice bred from *Kcne2*$^{+/-}$ dams; similar results were observed in 4/4 mice evaluated. *Left*, exemplar necropsy showing cardiomegaly; *center and right*, exemplar Masson's trichrome-stained LV showing fibrosis (blue). Scale bars: *center*, 100 μm; *right*, 30 μm.

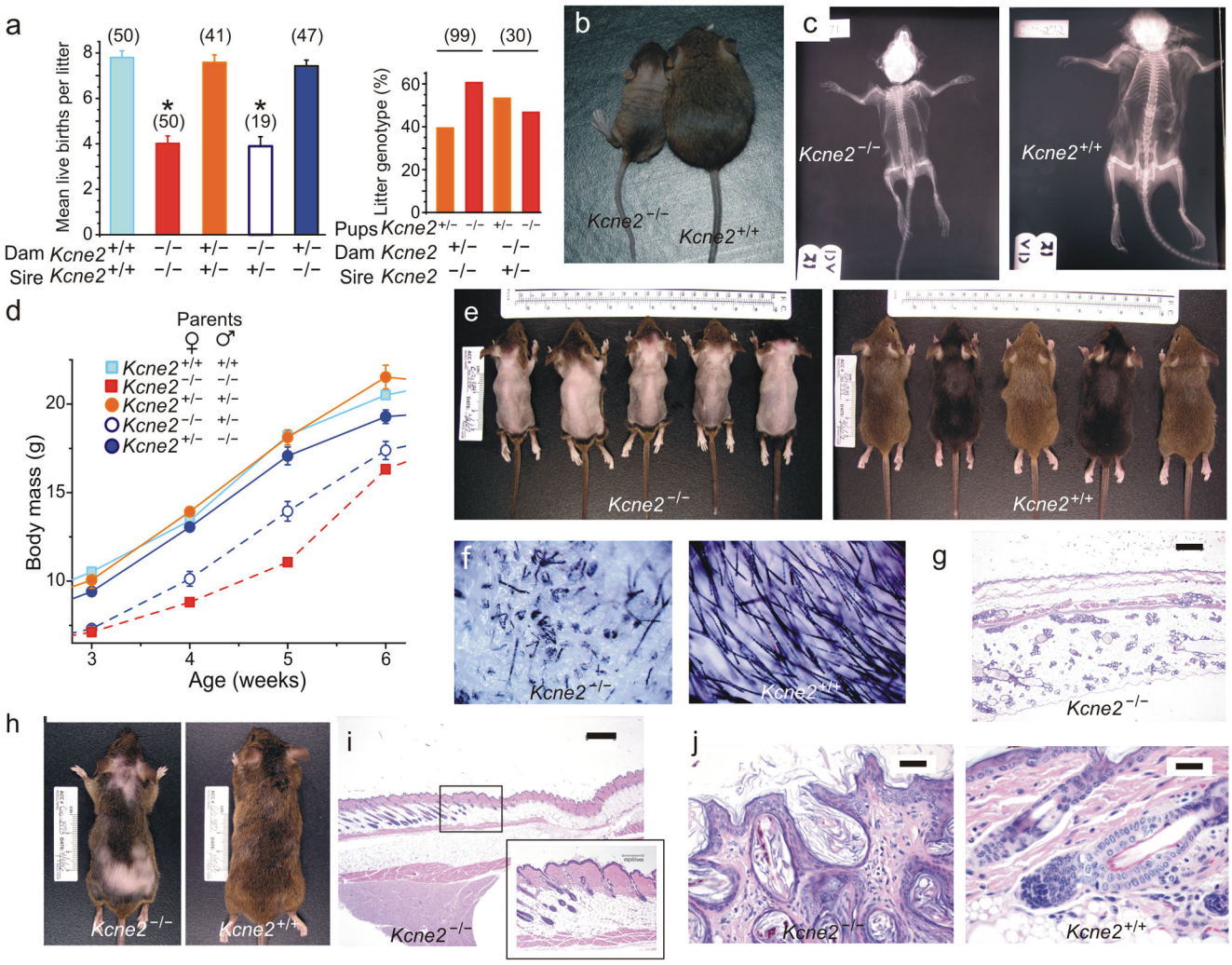

Figure 2. *Kcne2* disruption causes embryonic lethality, dwarfism and alopecia

(**a**) *Left*, mean live births per litter for wild-type and *Kcne2*-disrupted crosses as indicated; *n* = 19–50 litters per group. **P*<0.01. *Right*, genotype of surviving pups (%). *n* shown in parentheses.

(**b**) Exemplar 3-week-old pups from $Kcne2^{-/-} \times Kcne2^{-/-}$ and $Kcne2^{+/+} \times Kcne2^{+/+}$ crosses.

(**c**) Exemplar X-ray images of 5-week-old pups from $Kcne2^{-/-} \times Kcne2^{-/-}$ and $Kcne2^{+/+} \times Kcne2^{+/+}$ crosses.

(**d**) Mean body mass at 3–6 weeks of age for pups from wild-type and *Kcne2*-disrupted crosses as indicated; *n* = 15–50 pups per group. **P*<0.05.

(**e**) Exemplar 5-week-old $Kcne2^{+/+}$ and $Kcne2^{-/-}$ mice from homozygous crosses.

(**f**) Exemplar close-up views of skin from mice as in panel e.

(**g**) Exemplar micrographs of H&E-stained dermis sections from $Kcne2^{-/-}$ mouse as in panel e. Scale bar = 300 μm.

(**h**) Exemplar 1-year-old $Kcne2^{+/+}$ and $Kcne2^{-/-}$ mice from $Kcne2^{+/-} \times Kcne2^{+/-}$ crosses.

(**i**) Exemplar micrograph of H&E-stained dermis sections from *Kcne2*$^{-/-}$ mouse in panel i. *inset*, detail from boxed region, showing border zone between normal hair and alopecia, with abrupt cessation of mature hair follicles. Scale bar = 600 μm.
(**j**) H&E-stained sections showing hair follicles in dermis from *Kcne2*$^{+/+}$ and *Kcne2*$^{-/-}$ mice as in panel i. Scale bars = 20 μm.

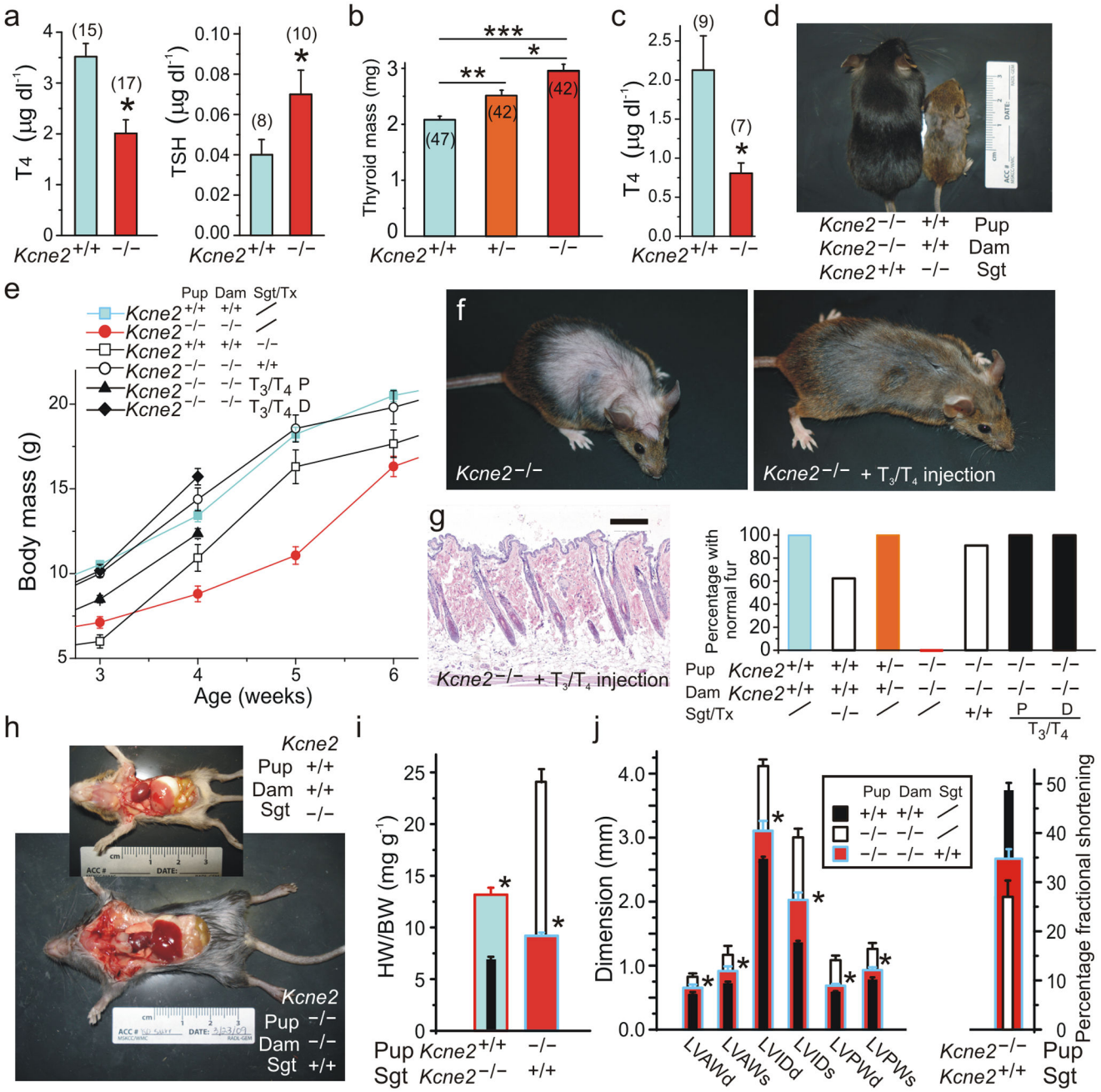

Figure 3. ***Kcne2*$^{-/-}$ mice are hypothyroid and treatable with T_3/T_4 or wild-type surrogacy**

(**a**) *Left*, Serum T_4 in *Kcne2*$^{+/+}$ & *Kcne2*$^{-/-}$ mice at 3 wks. *Right*, serum TSH in *Kcne2*$^{+/+}$ & *Kcne2*$^{-/-}$ mice at 3 wks. *significantly different from *Kcne2*$^{+/+}$ by ANOVA, $P < 0.001$. Numbers in parentheses indicate *n*.

(**b**) Mean mass of thyroid glands from 12 month old *Kcne2*$^{+/+}$, $^{+/-}$ and $^{-/-}$ mice from *Kcne2*$^{+/-}$ × *Kcne2*$^{+/-}$ crosses, weighed most-mortem, numbers in parentheses indicate *n*. Significant differences: * $P < 0.005$; ** $P < 1 \times 10^{-4}$; ***$P < 1 \times 10^{-9}$.

(**c**) Serum T_4 in pregnant *Kcne2*$^{+/+}$ & *Kcne2*$^{-/-}$ mice. *significantly different from *Kcne2*$^{+/+}$, $P < 0.001$.

(**d**) Exemplar 3-week-old pups from homozygous crosses surrogated (Sgt) with dams of opposite genotype

(**e**) Mean body mass at 3–6 weeks of age for pups from wild-type and *Kcne2*-disrupted crosses surrogated (Sgt), or treated (Tx) with T_3/T_4 injection (P) or by T_4 supplementation of their mothers (D); n = 9–23 pups per group. Untreated groups (/) from Figure 2 d shown for comparison.

(**f**) Exemplar 12-week-old *Kcne2*$^{-/-}$ mouse before (*left*) and after (*right*) 10 days QOD T_3/T_4 administration. Results were consistent in 5/5 mice evaluated.

(**g**) *Left*, histology of mouse in panel f after T_3/T_4 treatment showing recovery of normal hair follicles. Scale bar = 200 μm. *Right*, percentage of mice with normal hair growth grouped according to parental genotype. Groups were untreated (/), surrogated (Sgt) with dams (genotype as indicated) or treated (Tx) directly by QOD T_3/T_4injection (P) or by T_4 supplementation of their mothers (D); n = 16–23 mice per group.

(**h**) Exemplar necropsies of 3-week-old *Kcne2*$^{+/+}$ and *Kcne2*$^{-/-}$ mice bred from homozygous crosses, with/without surrogacy with mothers of opposite genotype.

(**i**) Mean heart weight/bodyweight (HW/BW; mg/g) for mice as in panel h, n = 7–9. *P<0.05 compared to values for non-surrogated pups (taken from Fig. 1c, key in Fig. 3j).

(**j**) Mean echocardiographic parameters for 3-week-old *Kcne2*$^{+/+}$ and *Kcne2*$^{-/-}$ mice bred from homozygous crosses, with/without surrogacy with mothers of opposite genotype. d/s, diastolic/systolic; LVAW, left ventricular anterior wall thickness; LVID, left ventricular internal diameter; LVPW, left ventricular posterior wall thickness, n = 5 mice. *P<0.05 compared to values for non-surrogated pups (taken from Fig. 1c).

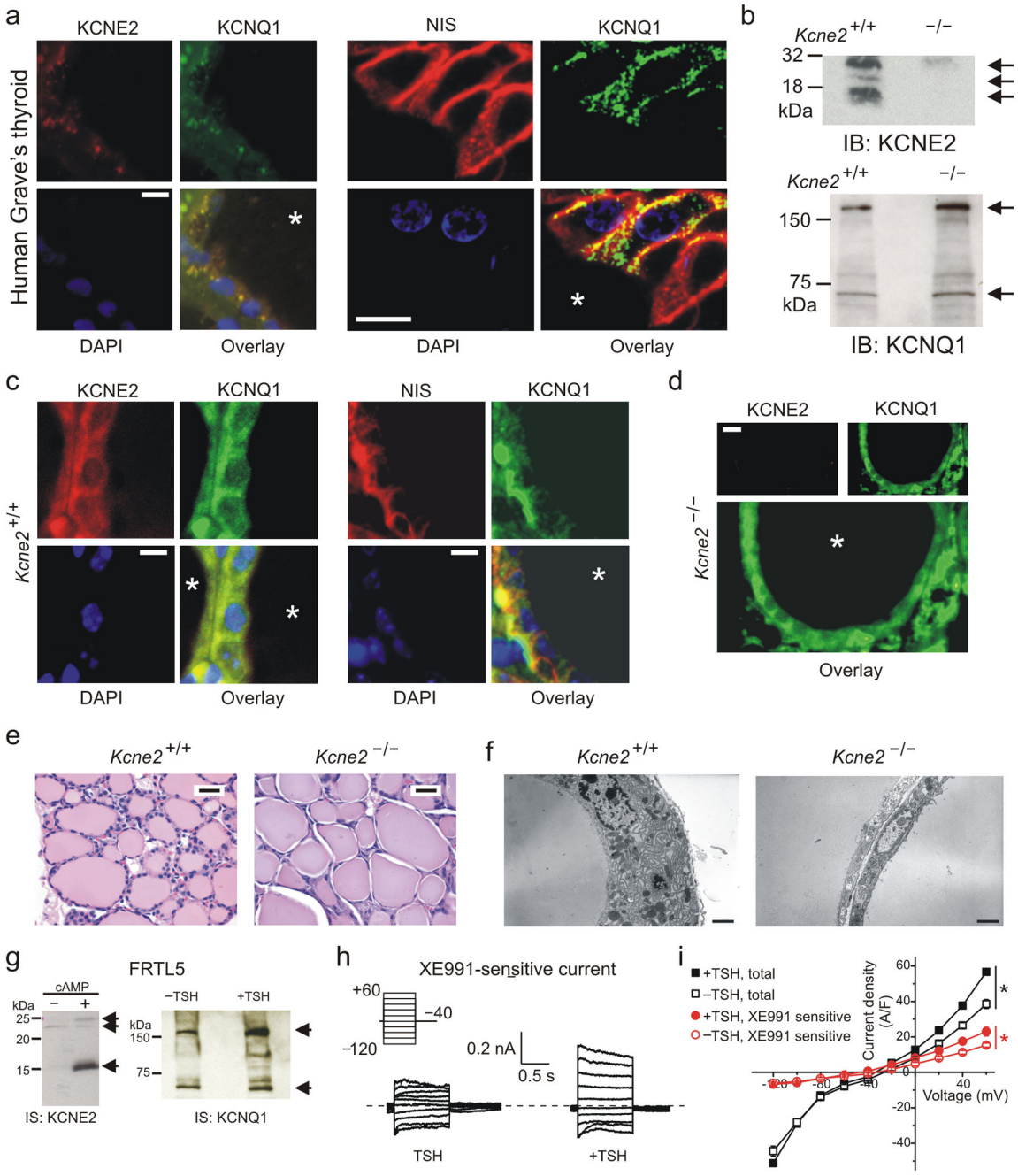

Figure 4. KCNE2 and KCNQ1 form a TSH-stimulated thyrocyte K^+ channel

(**a**) Immunofluorescence using antibodies raised against KCNE2, KCNQ1 and NIS in human thyrocytes in sections from individuals with Grave's Disease. DAPI visualization of nuclei shown in blue. *Colloid. Scale bars: 4 μm.

(**b**) Western immunoblots (IB) using antibodies raised against KCNE2 (arrows indicate the three glycosylation states of KCNE2) and KCNQ1 (lower arrow, monomer; upper arrow, multimer) in thyroid tissue from *Kcne2*$^{+/+}$ and *Kcne2*$^{-/-}$ mice (from *Kcne2*$^{+/-}$ × *Kcne2*$^{+/-}$ crosses).

(**c**) Immunofluorescence using antibodies raised against KCNE2, KCNQ1 and NIS, in thyrocytes of 3-month-old *Kcne2*$^{+/+}$ mice (from *Kcne2*$^{+/-}$ × *Kcne2*$^{+/-}$ crosses). *Colloid. Scale bars: 4 −μm.

(**d**) Immunofluorescence using antibodies raised against KCNE2 and KCNQ1, in thyrocytes of 3-monthold *Kcne2*$^{-/-}$ mice (from *Kcne2*$^{+/-}$ × *Kcne2*$^{+/-}$ crosses). *Colloid. Scale bars: 4 μm.

(**e**) H & E staining of adult *Kcne2*$^{+/+}$ and *Kcne2*$^{-/-}$ thyroid glands (from *Kcne2*$^{+/-}$ × *Kcne2*$^{+/-}$ crosses); scale bars, 20 μm.

(**f**) Electron micrographs of thyroid epithelium from adult *Kcne2*$^{+/+}$ and *Kcne2*$^{-/-}$ mice (from *Kcne2*$^{+/-}$ × *Kcne2*$^{+/-}$ crosses). Scale bars, 2 μm.

(**g**) Western blots of membrane fractions from FRTL5 cells with and without 10 hours incubation with cAMP, using antibodies raised against KCNE2 (arrows putatively indicate the three predicted glycosylation states); and FRTL5 cells with and without 6 days TSH incubation, using antibodies raised against KCNQ1 (lower arrow, monomer; upper arrow, tetramer).

(**h**) Exemplar whole-cell patch-clamp recordings of XE991-sensitive currents in FRTL5 cells with or without TSH incubation. Upper left inset: voltage protocol. Zero current level indicated by dashed line.

(**i**) Mean whole-cell total (n = 9–16) and XE991-sensitive (n = 8–9) current relationships for FRTL5 cells with or without TSH incubation. Significant difference: *$P < 0.05$.

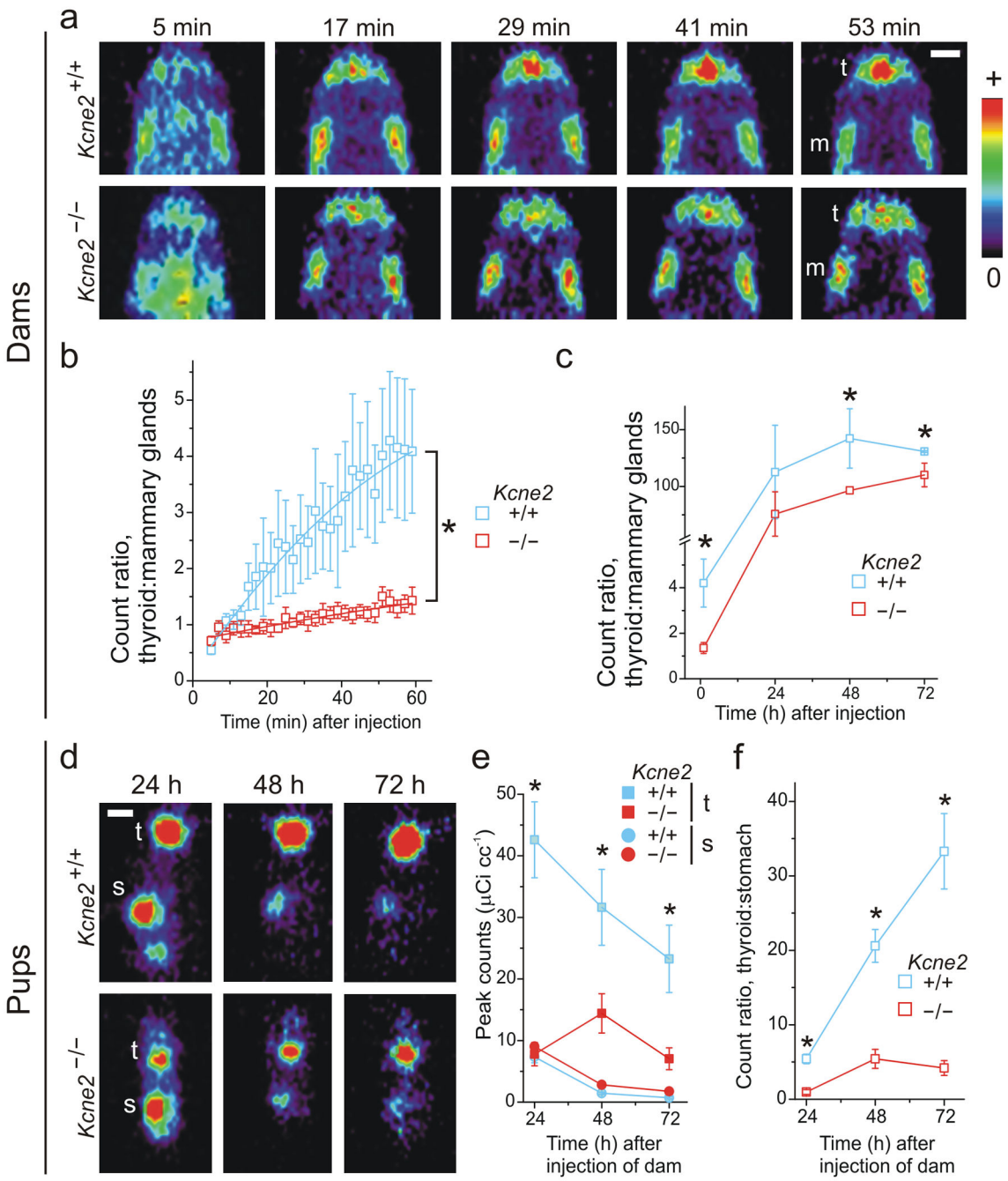

Figure 5. *Kcne2* is required for normal thyroid I^- accumulation

(**a**) Exemplar microPET images of lactating *Kcne2*$^{+/+}$ and *Kcne2*$^{-/-}$ dams recorded during the first hour after tail vein injection of ^{124}I. Labels: t, thyroid; m, mammary glands. Color intensity scale on right, showing red indicates highest intensity. Scale bar (white) = 5 mm. (**b**) Mean ^{124}I accumulation in thyroid relative to mammary gland from imaging as in panel a, $n = 4$ mice per group, error bars indicate SEM. Measured as ratio of maximum radioactivity in each tissue minus mean background count in each mouse. *$P<1\times10^{-8}$.

(**c**) Mean ^{124}I accumulation in thyroid relative to mammary gland as in panel a but from 1–72 hours after tail vein injection of ^{124}I, n = 4–5 mice per group, error bars indicate SEM. *P<0.05.

(**d**) Exemplar microPET images of pre-weaning *Kcne2*$^{+/+}$ and *Kcne2*$^{-/-}$ pups recorded 24–72 hours after their mothers (same dams as in panels a–c) received tail vein injections of ^{124}I. Labels: t, thyroid; s, stomach. Intensity scale as in panel a. Scale bar (white) = 5 mm.

(**e**) Mean ^{124}I accumulation (in μCi) in thyroid and stomach from imaging as in panel d, n = 7–12 pups per time-point per group, error bars indicate SEM. Measured as maximum radioactivity in each tissue minus mean background count in each mouse. *P<0.05.

(**f**) Mean ^{124}I accumulation in thyroid relative to stomach, imaging method and pups as in panel e. Measured as ratio of maximum radioactivity in each tissue minus mean background count in each mouse. *P<0.0005.

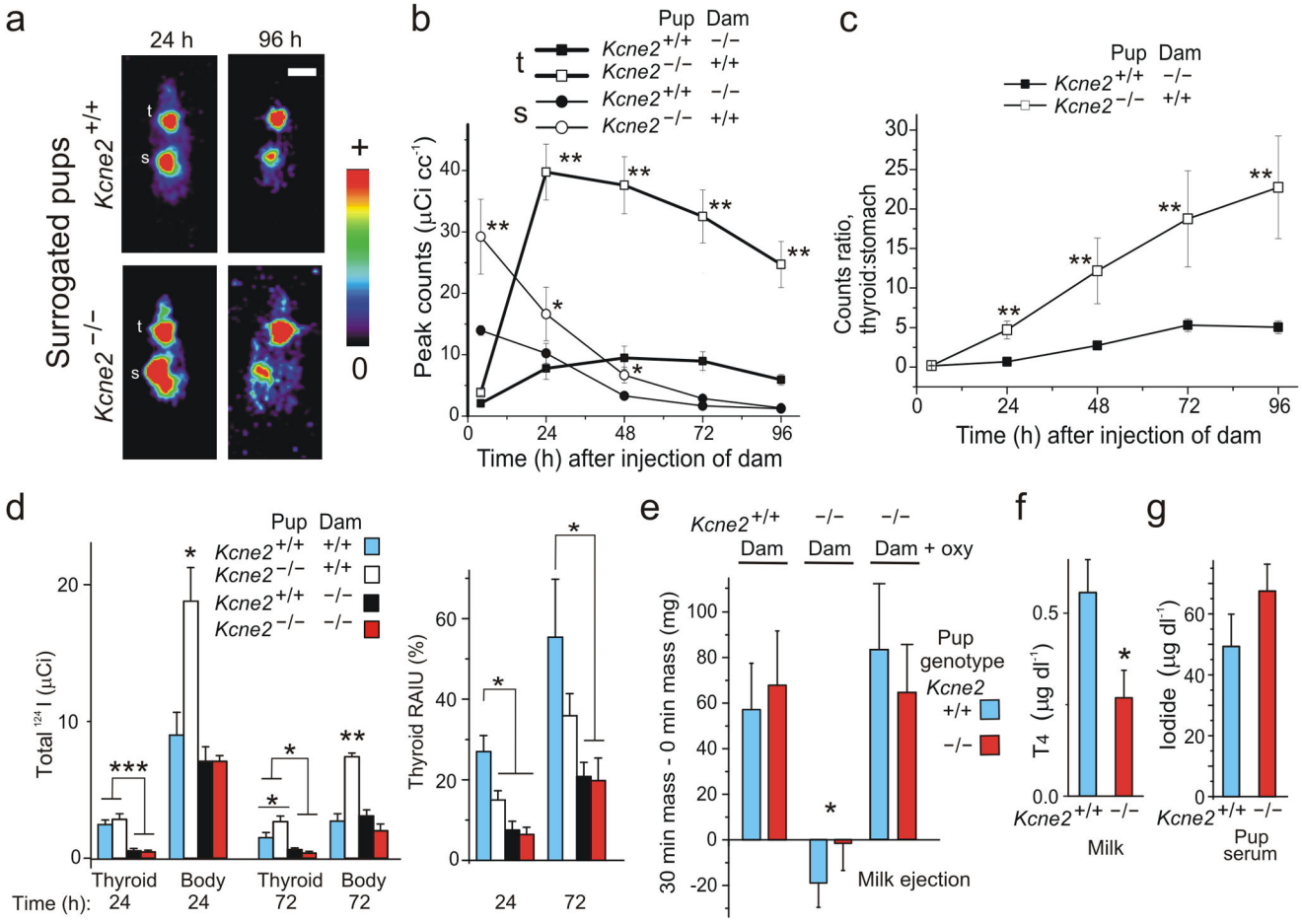

Figure 6. *Kcne2*$^{-/-}$ dams have a milk ejection defect and produce low-T_4 milk

(**a**) Exemplar microPET images of pre-weaning *Kcne2*$^{+/+}$ and *Kcne2*$^{-/-}$ pups recorded 24–96 hours after their surrogate mothers of opposite genotype received tail vein injections of ^{124}I. Labels: t, thyroid; s, stomach. Intensity scale shown on right. Scale bar (white) = 10 mm.

(**b**) Mean peak ^{124}I accumulation (measured as peak µCi cc^{-1}) in thyroid and stomach from imaging as in panel a, *n* = 7–12 pups per time-point per group, error bars indicate SEM. Measured as maximum radioactivity in each tissue minus mean background count in each mouse. **P*<0.05; ***P*<0.01.

(**c**) Mean peak ^{124}I accumulation in thyroid relative to stomach, imaging method and pups as in panel a. Measured as ratio of maximum radioactivity in each tissue minus mean background count in each mouse. ***P*<0.001.

(**d**) Effects of pup and dam genotype on pup *total* thyroid and body ^{124}I accumulation (*left*), and thyroid RAIU (radioactive iodide uptake as a percentage of total body radioiodine) (*right*), determined using 3D regions of interest from PET analyses of pup ^{124}I accumulation (surrogated and non-surrogated) after tail vein injection of dams; *n* = 7–12. **P*<0.05; ***P*<0.005; ****P*<0.0005.

(**e**) Milk ejection assay. Mean mass of pups before (0 min) and after 30 min feeding period; $n = 8–20$; *$P<0.01$. 'oxy' indicates dams injected with oxytocin 10 minutes prior to feeding period.

(**f**) Milk T_4 concentration; $n = 5–7$; *$P<0.05$.

(**g**) Plasma I^- concentration in 3-week-old pups; $n = 6$ per genotype.